A&A 422, L63–L66 (2004)
DOI: 10.1051/0004-6361:200400019

Astronomy & Astrophysics

Letter to the Editor

Brightness and size of small-scale solar magnetic flux concentrations

E. Wiehr[1], B. Bovelet[1], and J. Hirzberger[2]

[1] Universitäts-Sternwarte, Geismarlandstraße 11, 37083 Göttingen, Germany
e-mail: ewiehr@uni-sw.gwdg.de
[2] Institut für Geophysik, Astrophysik und Meteorologie, Universitätsplatz 5, 8010 Graz, Austria

Received 13 April 2004 / Accepted 22 June 2004

Abstract. The new 1 m Swedish Solar Telescope SST on La Palma allows to observe inter-granular *G*-band bright points (igBP) in solar active regions at an unprecedented spatial resolution. The igBP are reasonably assumed to be small-scale magnetic flux-concentrations. A sample of more than 1500 igBP shows tight relations of diameter and brightness in the *G*-band and in the continuum; it covers a diameter range of 100 km to 300 km, with a most frequent value near 160 km. Features larger than 300 km formerly reported, evidently result from insufficient spatial resolution; that upper diameter limit is close to the typical width of inter-granular lanes, and suggests a "gap" to small pores. The lack of igBP with sizes below 130 km is discussed not to arise from the finite spatial resolution of the 1 m telescope.

Key words. Sun: photosphere – magnetic fields

1. Introduction

The solar surface is widely covered by small magnetic flux concentrations, even outside active regions and in the minimum of the solar cycle. The true size and the magnetic flux of these features are still subject of scientific debate (Keller 1992; Sánchez Almeida 2000); another interesting question concerns the physical difference of bright and dark magnetic regions. A precise investigation of magnetic regions requires high spatial resolution Zeeman polarimetry (e.g., Domínguez Cerdeña et al. 2003) which, however, implies additional optical surfaces in the instrumental setup and diminishes the instrument's efficiency and the spatial resolution. Small-scale magnetic flux-concentrations can also be identified using their brightness excess in the 430 nm absorption lines of the CH molecule (e.g., Muller & Roudier 1984; Title & Berger 1996) which allows the use of filters instead of a spectrograph, yielding short exposure times and thus high spatial resolution (cf. Fig. 1).

The *G*-band bright points (BP) mark either magnetic or non-magnetic structures (Berger & Title 2001); Langhans et al. (2002) identified the former as inter-granular downdraft motions, and the latter as granular edges with upward motions. For an automatic separation of both, Bovelet & Wiehr (2003) applied a "local contrast criterion" making use of the larger contrast of magnetic structures to their inter-granular surroundings compared to non-magnetic ones. The thus identified inter-granular *G*-band bright points (hereafter referred to as "igBP") were used as tracers for small-scale magnetic flux-concentrations. Here, we present a study of small-scale inter-granular *G*-band bright points at unprecedented spatial resolution.

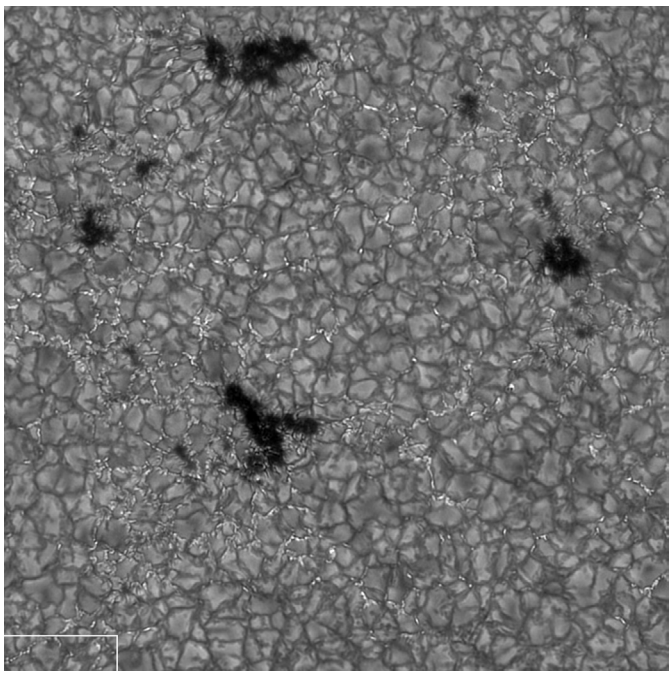

Fig. 1. Speckle reconstructed *G*-band image of an active region at 9°N, 8°W, taken with the 1 m SST on July 14, 2003; field of view: 57 arcsec × 57 arcsec; the lower left rectangle marks the sub-field in Fig. 2.

2. Observations

We used the new 1 m Swedish Solar Telescope on La Palma (SST; Scharmer et al. 2003) on July 14 and 15, 2003, to observe active regions near the solar disk center. Images in the "*G*-band" at 430.5 ± 1 nm were simultaneously taken with continuum images at 587.5 ± 1 nm. The tip-tilt mirror of the SST assured an effective correction for influences of image motion. Bursts of some dozens of images each integrated over 4 ms in the *G*-band and, respectively, 7 ms in the continuum were processed using the speckle-masking method (Pelemann & von der Lühe 1989; de Boer 1996). For a comparison of the reconstructed images in *G*-band and 587 nm continuum, the latter were destreched using a "local correlation tracking algorithm" (November & Simon 1988). Finally, the pattern recognition algorithm of Bovelet & Wiehr (2001) was applied to the reconstructed *G*-band image to automatically detect features brighter than the mean ambient photosphere (BP). The 1528 *intergranular* ones among these *G*-band bright points were finally selected (cf. Fig. 2) using the above mentioned local contrast criterion (Bovelet & Wiehr 2003). We tuned our algorithm in such a manner that bright granular edges were certainly excluded, even at the price of loosing some igBP.

In order to compare the *G*-band with the corresponding continuum image, we apply our pattern recognition to the *continum image completely independent from the G-band* analysis – this time without any selection criterion, since the small-scale inter-granular features do not show a pronounced continuum intensity excess. The thus identified continuum structures include numerous tiny features such as granular fragments, minigranules, granular sub-structures, but also the (magnetic) "solar filigree" (Dunn & Zirker 1973). Among these, we selected the inter-granular structures exclusively by spatial correspondence with the *G*-band-selected igBP sample, thus obtaining *diameter and mean brightness independently from the G-band analysis*.

Our algorithm assigns to each feature a specific size, given by the area of the covered pixels, avoiding any explicit assumption for fitting an intrinsic intensity profile. We set the lower detection limit to 9 pixels, e.g. 3×3 pixels (far from the Nyquist limit) corresponding to $0.123'' \times 0.123''$ (91 km × 91 km in July). We then approximate each igBP feature by a corresponding ellipse of equal area, and establish that the majority of igBP is largely circular (cf. Berger et al. 1995; Bovelet & Wiehr 2003). We assign to each structure the diameter D of a circle covering the same area.

3. The brightness of igBP

Our simultaneous imaging of inter-granular small-scale features allows to compare their brightness in the *G*-band and continuum. Brightest igBP exceed the mean photospheric intensity up to a factor of 1.8 in *G*-band and 1.3 in the continuum; this agrees with findings by (Sánchez Almeida et al. 2001). We find a remarkably tight relation between both intensities with a gradient 2.4 (Fig. 3), in agreement with empirical models (Sánchez Almeida et al. 2001).

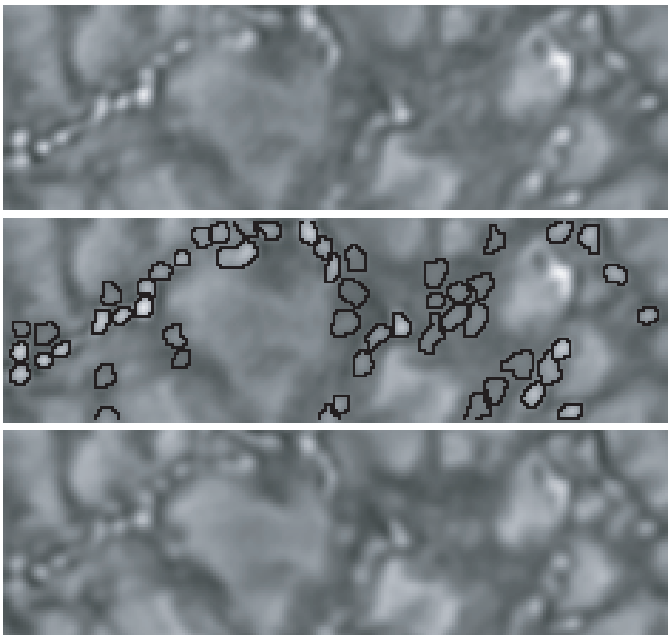

Fig. 2. Speckle reconstructed *G*-band (*upper*) and simultaneous 587 nm continuum (*lower*) images of a 9.6 arcsec × 3.0 arcsec (7.1 Mm × 2.2 Mm) sub-field (rectangle at the lower left in Fig. 1); the middle panel shows the segmentated inter-granular features recognized in the *G*-band image (including even faintest ones for the tests explained in 4.2.b).

When plottting the intensity of each igBP versus its size (Fig. 4), we find a largely flat relation showing that the igBP exhibit a *mean* brightness excess, almost independent from their size. The slight intensity decrease below 140 km stays within the 1 σ width of the igBP brightness range and agrees with previous findings (Berger et al. 1995; Bovelet & Wiehr 2003).

4. The diameter of igBP

Our simultaneous imaging in *G*-band and continuum allows to compare the diameters of inter-granular small-scale features in both formation heights. We find (Fig. 5) that the sizes of the igBP are largely equal; deviations from the 45° line may readily be caused by slightly different intensity "trends" over the two images. These let the pattern recognition algorithm segmentate slightly different contours (a few pixels) on its given intensity thresholds. The poorer spatial resolution of in the 587 nm continuum as compared to the 430 nm *G*-band can be seen as a somewhat higher data point above the 45° line in Fig. 5. Our finding of equal diameters in the *G*-band and the continuum indicates a rather small difference in formation height and supports that the recognized features are real.

In Fig. 6, we present the size histogram for igBP segmentated in *G*-band. It shows a narrow range between 100 km and 300 km with a most frequent diameter of 160 ± 20 km, in good agreement with the 150 km fluxtubes obtained from indirect line-ratio measurements (Stenflo 1973; Wiehr 1978).

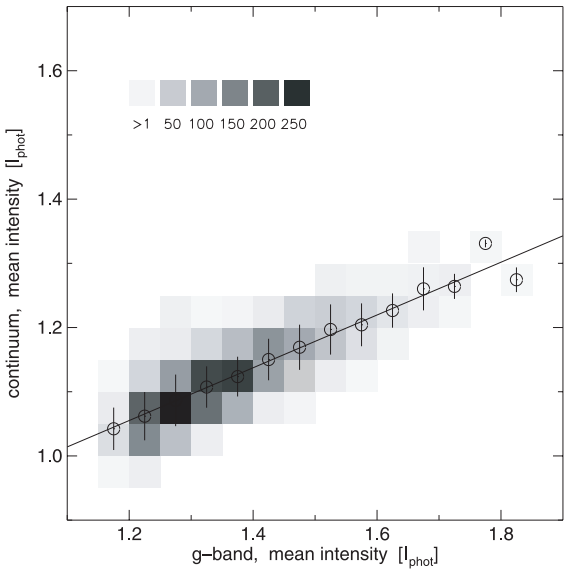

Fig. 3. Two dimensional histogram of the mean intensity of 1528 inter-granular bright points recognized in the *G*-band (abscissa) and in the continuum image (ordinate); the gray-scales give the number density of each data point; circles give the weighted means, vertical bars the $\pm 1\sigma$ deviations.

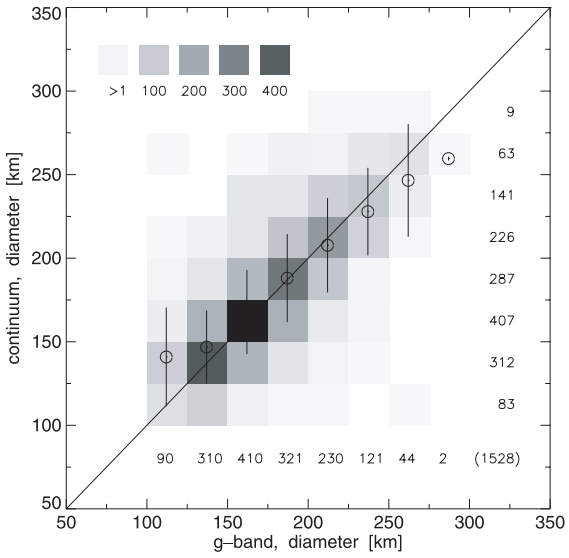

Fig. 5. Two dimensional diameter histogram of 1528 inter-granular bright points recognized in the *G*-band (abscissa) and in the continuum image (ordinate); the gray-scales give the lower boundary of the number density intervals; the total numbers of igBP for each sizebin is indicated; circles give the weighted means, vertical bars the $\pm 1\sigma$ deviations.

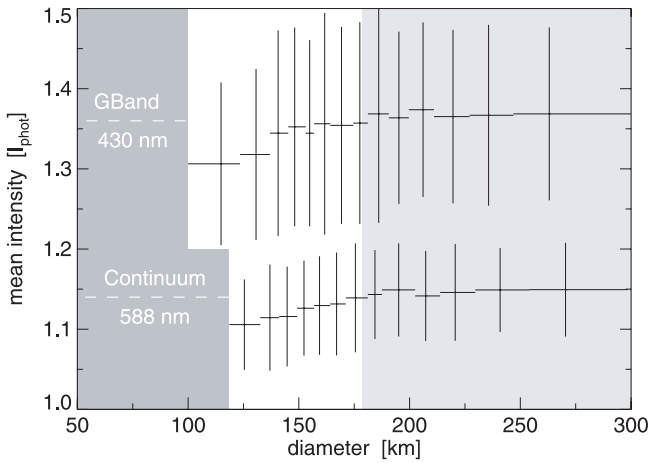

Fig. 4. Intensity-diameter relation of inter-granular features recognized in the *G*-band (upper) and in the continuum (lower part); *x*-bars mark samples of equal statistical weight; *y*-bars give standard deviations; light grey indicates the resolution range of an ideal 45 cm telescope; dark grey visualizes sizes below the SST's resolution; dotted lines give the total means.

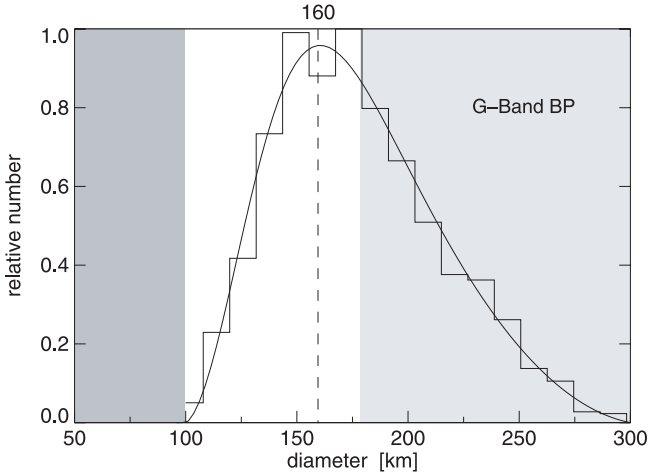

Fig. 6. Diameter histogram for 1528 inter-granular *G*-band bright points fitted by a polynomial; light grey indicates the resolution range of an ideal 45 cm telescope; dark grey visualizes sizes beyond the resolution limit achieved.

4.1. The upper size limit

We find no structures larger than 300 km: the high spatial resolution of the 1 m SST allows a separation of structures which appear elongated at less spatial resolution (forming "filigree crincles"; cf. Dunn & Zirker 1973). Indeed, *G*-band images with less resolution yield igBP with larger diameters having the same mean brightness as in Fig. 4 – as expected for clusters of unresolved smaller igBP.

Our upper size limit near 300 km is close to the typical width of mean inter-granular lanes. This suggests that the corresponding flux-concentrations are "squeezed" by neighboring granules (Muller & Roudier 1992), thus being elongated and fitting the inter-granular spacings. Such features ("filigree crincles") might finally split due to inter-change instabilities (e.g. Schüssler 1984; Bünte 1993). Indeed, careful inspection of time series (Bovelet & Wiehr 2003) shows that chains of igBP mostly reveal splitting processes.

A maximum diameter of $D \approx 300$ km corresponds to a magnetic flux of about 10^{18} Mx for a field of 1500 G; this value might be lower if the filling of magnetic field within an igBP is smaller than unity. At higher magnetic flux, solar magnetic regions appear dark. Calculations for the stability of sunspots (Meyer et al. 1977) indicate a lower limit of the sunspot magnetic flux near 10^{19} Mx, being ten times above the upper flux

limit for igBP. Assuming 2000 G magnetic field strength for small dark features 10^{19} Mx would correspond to diameters of 800 km, which seems a reasonable value for small pores (e.g., Hirzberger 2003).

4.2. The lower size limit

The decrease of the number of igBP smaller than 130 km diameter is not an instrumental artifact; there is a true deficit of small igBP as inferred from Fig. 6. Our claim is based on the following arguments:

a) The smallest igBP do not show an intensity significantly different from the rest. If smallest igBP were not sufficiently resolved in our data, these should appear fainter, since part of the observed light would come from their dark surroundings. However, such a significant brightness decrease is not seen in Fig. 4.
b) The finding that diameters of corresponding features are equal in the *G*-band and in the continuum image (Fig. 5), indicates that the deduced sizes are real.
c) The maximum of the histogram Fig. 6 does not vary, when including fainter igBP by successive reduction of the minimum brightness. If smallest features were systematically fainter, their increasing contribution to the histogram should shift the maximum. This is not found, implying that even our faint igBP are still sufficiently above SST's resolution limit, the maximum thus being real.
d) The decrease of the number of igBP diameters in Fig. 6 appears significantly above SST's resolution limit (85 km; cf. Scharmer et al. 2003) and extends over several diameter binnings. If that decrease would be an artifact of the limited resolution (even for speckle reconstructed images), we should expect a similar finding for the DOT data; Bovelet & Wiehr (2003), however, find a sharp histogram cut at their actual 180 km resolution limit (marked light gray in our Figs. 4 and 6). A fall-off in the histogram by Berger et al. (1995) almost coincides with their theoretical resolution limit of 130 km.

5. Conclusions

We find that igBP appear with diameters covering a limited range between 100 km and 300 km. The decrease near 130 km (Fig. 6) is close to the photon mean free path in the photosphere, so that smaller features would be laterally optical thin and therefore difficult to detect. The upper diameter limit indicates a gap between 10^{18} Mx and 10^{19} Mx for bright and dark flux-concentrations; indeed, the intensity–diameter relation (Fig. 4) gives no indication for a "smooth transition" to dark magnetic structures (Spruit & Zwaan 1985; Knölker & Schüssler 1988; Soltau 1997). The bright magnetic flux-concentrations may then be intrinsically different from dark solar magnetic structures, all the more igBP show strong lateral motions (e.g., Bovelet & Wiehr 2003) in contrast to dark pores which may be deeper rooted.

Acknowledgements. We thank Drs. G. Scharmer and D. Kiselman for their kind support with the SST, Dr. J. Sánchez Almeida for valuable suggestions, and Drs. O. von der Lühe, M. Schüssler, F. Hessman for helpful discussions. The SST is operated by the Swedish Academy of Sciences at the Spanish Observatorio del Roque de los Muchachos (IAC). The data processing was done at the Institut für Geophysik, Astrophysik und Meteorologie Graz (IGAM) and at the Gesellschaft für wissenschaftliche Datenverarbeitung Göttingen (GWdG).

References

Berger, T. E., & Title, A. M. 2001, ApJ, 553, 449
Berger, T. E., Shrijver, C. J., Shine, R. S., et al. 1995, ApJ, 454, 531
Bovelet, B., & Wiehr, E. 2001, Sol. Phys., 201, 13
Bovelet, B., & Wiehr, E. 2003, A&A, 412, 249
Bünte, M. 1993, A&A, 276, 236
de Boer, C. R. 1996, A&AS, 120, 195
Domínguez Cerdeña, I., Sánchez Almeida, J., & Kneer, F. 2003, A&A, 407, 741
Dunn, R. B., & Zirker, J. B. 1973, Sol. Phys., 33, 281
Grossmann-Doert, U., Knölker, M., Schüssler, M., & Solanki, S. 1994, A&A, 285, 648
Hirzberger, J. 2003, A&A, 405, 331
Keller, C. U. 1992, Nature, 359, 307
Knölker, M., & Schüssler, M. 1988, A&A, 194, 257
Langhans, K., Schmidt, W., & Tritschler, A. 2002, A&A, 394, 1069
Meyer, F., Schmidt, H. U., & Weiss, N. O. 1977, MNRAS, 179, 420
Muller, R., & Roudier, T. 1984, Sol. Phys., 94, 33
Muller, R., & Roudier, T. 1992, Sol. Phys., 141, 27
November, L. J., & Simon, G. W. 1988, ApJ, 333, 427
Pehlemann, E., & von der Lühe, O. 1989, A&A, 216, 337
Sánchez Almeida, J. 2000, ApJ, 544, 1135
Sánchez Almeida, J., Asensio Ramos, A., Trujillo Bueno, J., & Cernicharo, J. 2001, ApJ, 555, 978
Scharmer, G. B., Bjelksjo, K., Korhonen, T., K., Lindberg, B., & Pettersen, B. 2003, Proc. SPIE, 4853, 370
Schüssler, M. 1984, A&A, 140, 453
Soltau, D. 1997, A&A, 3117, 586
Spruit, H. C., & Zwaan, C. 1981, Sol. Phys., 70, 207
Stenflo, J. 1973, Sol. Phys., 32, 41
Title, A. M., & Berger, T. E. 1996, ApJ, 463, 797
Wiehr, E. 1978, A&A, 69, 279